

Quantum spin liquid phase in the Shastry-Sutherland model detected by an improved level spectroscopic method

Ling Wang,^{1,*} Yalei Zhang,² and Anders W. Sandvik^{3,4,†}

¹*Department of Physics, Zhejiang University, Hangzhou 310000, China*

²*Beijing Computational Science Research Center, 10 East Xibeiwang Road, Beijing 100193, China*

³*Department of Physics, Boston University, 590 Commonwealth Avenue, Boston, Massachusetts 02215, USA*

⁴*Beijing National Laboratory for Condensed Matter Physics and Institute of Physics, Chinese Academy of Sciences, Beijing 100190, China*

(Dated: June 14, 2022)

We study the spin-1/2 two-dimensional Shastry-Sutherland spin model by exact diagonalization of clusters with periodic boundary conditions. We develop an improved level spectroscopic technique using energy gaps between states with different quantum numbers. The crossing points of some of the relative (composite) gaps have much weaker finite-size drifts than the normally used gaps defined only with respect to the ground state, thus allowing precise determination of quantum critical points even with small clusters. Our results support the picture of a spin liquid phase intervening between the well known plaquette-singlet and antiferromagnetic ground states, with phase boundaries in almost perfect agreement with a recent density matrix renormalization group study, where much larger cylindrical lattices were used [J. Yang et al., Phys. Rev. B **105**, L060409 (2022)]. The method of using composite low-energy gaps to reduce scaling corrections has potentially broad applications in numerical studies of quantum critical phenomena.

Introduction.—Quantum spin liquids (QSLs) [1] are some of the most intriguing phases of two-dimensional (2D) quantum matter, yet they have been experimentally elusive. The kagome Heisenberg antiferromagnet and the Kitaev honeycomb model are among the most well studied examples. The former hosts a QSL ground state whose nature was debated for years [2] but now is largely settled as a gapless variant [3, 4]. The latter has exactly solvable gapped and gapless QSL phases [5]. Both models have attracted enormous attention because of their possible experimental realizations in layered quantum magnets [6–8]. Recent experiments support gapless QSLs in both kagome [9, 10] and honeycomb systems [11, 12]. Here it should be noted that various defects and disorder can drastically influence gapless excitations and drive quantum magnets to randomness-dominated quantum states completely different from the conjectured pristine gapless QSLs [13–15]. Experimentally, it is often difficult to distinguish between these states, as exemplified by contradictory studies of triangular-lattice systems [16–18]

Another prominent quasi-2D frustrated quantum magnet is SrCu₂(BO₃)₂ (SCBO) [19–26], whose in-plane copper magnetic exchange and super-exchange integrals realize the interdimer (J) and intra-dimer (J') interactions of the spin-1/2 Shastry-Sutherland model (SSM) [27], illustrated in Fig. 1(a). Under increasing hydrostatic pressure, the ratio $g \equiv J/J'$ increases, and the material undergoes transitions among the three well established ground state phases of the SSM; the dimer singlet (DS) phase, a plaquette-singlet solid (PSS) phase, as well as an antiferromagnetic (AFM) phase [19–26].

Until recently, SCBO was not widely considered as a candidate for a QSL phase; instead the putative deconfined quantum critical point (DQCP) separating the PSS and AFM phases was the focus of theoretical studies of the SSM [28] and other models with PSS and AFM phases [29, 30]. However, a recent density matrix renormalization group (DMRG) study detected a gapless QSL state intervening between the PSS and

AFM phases of the SSM [31] within a narrow range of couplings, approximately $g \in (0.79, 0.82)$. Subsequently, an intervening phase with similar boundaries was also indicated by a functional renormalization-group calculation [32]. If these results are correct, they open the interesting possibility of a QSL phase also between the PSS and AFM phases in SCBO, somewhere in the pressure range 2.6 to 3.2 GPa, where experiments so far [25, 26] have not detected any conventional phase transitions or long-range order. This prospect of realizing a gapless QSL is especially important considering that SCBO can be synthesized with very low concentration of impurities, thus, it is free of the complicating disorder effects mentioned above.

The aim of the present work is to further corroborate the QSL phase argued in Ref. 31, where excited-state gaps computed with the DMRG method were analyzed. Gap crossings associated with quantum phase transitions were identified, similar to the previously studied J_1 - J_2 square-lattice Heisenberg model [33] (where several other works also agree on the

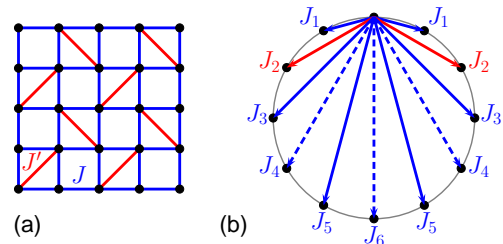


Figure 1. Illustration of the spin-1/2 models studied here. (a) The SSM, with blue and red lines indicating the Heisenberg AFM interactions J and J' , respectively. (b) Heisenberg spin chain with long-range interactions, with all couplings of one spin (top of the ring) to all the other spins marked according to the type of coupling. The blue solid and dashed lines mark unfrustrated AFM (odd distances) and ferromagnetic (even distances) couplings, respectively, and the red lines show the frustrated AFM J_2 interactions.

existence of a QSL in roughly the same coupling range [34–38]). Crossing points flowing with increasing system size to two different points were found, $g_{c1} \approx 0.79$ and $g_{c2} \approx 0.82$, and these were associated with transitions out of the PSS phase and into the AFM phase, respectively. The gaps and correlation functions in the window $[g_{c1}, g_{c2}]$ supported a gapless QSL phase between the PSS and AFM phases.

Here we develop an improved level-spectroscopy method, using combinations of excitation energies beyond the gaps with respect to the ground state. By judicious choices of quantum numbers and identification of composite and elementary excitations on fully periodic lattices, spectral gap combinations can be defined whose crossing points exhibit only very weak dependence on the lattice size. Even with the small clusters accessible with exact diagonalization, we can confirm crossing points in excellent agreement with those extrapolated from the conventional gap crossings in much larger systems with cylindrical boundary conditions [31]. To further demonstrate the improved gap crossing method, we also consider a spin chain with long-range interactions, illustrated in Fig. 1(b), which has a similar ground-state phase structure as a function of an exponent controlling the long-range couplings.

We also study the relevant order parameters of both models. The results further demonstrate the utility of the level crossing method to detect quantum phase transitions when the system sizes are too small to reliably extrapolate the order parameters to the thermodynamic limit.

Exact diagonalization and level crossings—Exact diagonalization of the Hamiltonian is the most versatile numerical method for quantum lattice models, however strongly limited to small lattice sizes owing to the prohibitive exponential growth of the Hilbert space. Proper selection of cluster sizes and shapes, and thorough examination of their lattice symmetries (conserved quantum numbers for block-diagonalization), are the two most important steps for fully utilizing the power of the method [39–43].

The quantum numbers are also important for understanding and exploiting excitations, which are useful not only in their own right but also for detecting phase transitions of the ground state. The underlying assumption of the level spectroscopic method that we will use here is that a change in the ground state at a quantum phase transition is also accompanied by a change in the elementary excitations, which can be reflected in a re-arrangement of energy levels with different quantum numbers. If that is the case, there will be real level crossings of excited states even when ground state transition takes place through an avoided level crossing (i.e., with the quantum numbers of the ground state on a finite cluster not changing versus the control parameter).

The level crossing method is very well known in the context of 1D models, especially the frustrated J_1 - J_2 Heisenberg chain where this approach originated [44, 45]. The power of the method in this case lies in the fact that the crossing point between the lowest singlet and triplet excitations versus J_2/J_1 converges very rapidly to the critical point with increasing chain length N , with shifts proportional to N^{-2} . Subleading

corrections are small, and the transition point can be obtained to precision 10^{-6} [45] or even better [43] even with chain lengths only up to $N = 32$, easily accessible with exact diagonalization. In other cases, e.g., the chain with long-range interactions that we will also consider here, the subleading corrections are more substantial but still reliable results can be obtained with relatively small chains [46].

More recently, the level-crossing approach has also been applied to 2D systems, in combination with a variety of methods for computing the relevant excited states, e.g., quantum Monte Carlo [47], DMRG [33], and sophisticated variational wave functions [36, 37]. In the previous application to the SSM [31], the DMRG method was used to generate excited states in several symmetry sectors on cylindrical lattices (i.e., with open boundaries in one lattice direction and periodic boundaries in the other direction). With fully periodic lattices, results converged to the degree necessary for reliable level-crossing studies are difficult to obtain with the DMRG method for system sizes much beyond those for which exact diagonalization (with, e.g., the Lanczos method) can be used. Periodic lattices are preferable, because of their higher symmetry, thus allowing access to additional quantum numbers beyond those used with the DMRG method. Here we will show that even very small periodic lattices already contain the spectral information pertaining to the ground state transitions of the SSM, but suitable gaps and combinations of gaps have to be identified.

The SSM Hamiltonian is

$$H = J \sum_{\langle ij \rangle} \mathbf{S}_i \cdot \mathbf{S}_j + J' \sum_{\langle ij \rangle'} \mathbf{S}_i \cdot \mathbf{S}_j, \quad (1)$$

where \mathbf{S}_i are $S = 1/2$ operators, $\langle ij \rangle$ in the J sum represents all nearest-neighbor site pairs on a 2D square lattice, and $\langle ij \rangle'$ in the J' sum indicates next-nearest neighbor sites belonging to one of the diagonal bonds in a given plaquette but only in every second plaquette, as illustrated in Fig. 1(a). As is customary, we will refer to the plaquettes with and without J' interaction as filled and empty, respectively.

We use the Lanczos method for periodic clusters with $N = 16, 20, 24, 28, 32, 36$; see Fig. 2. The $N = 40$ system is beyond the reach of the Lanczos method within our computational resources, but some of its low-energy states can be completely converged by the implementation of the DMRG method described in Ref. [31]. For larger fully periodic clusters, convergence of excited states to the degree we demand here also becomes too challenging for DMRG (in contrast to the much larger cylindrical lattices studied previously [28, 31]).

The specific Heisenberg chain with long-range interactions that we also study as a benchmark case is defined by

$$H = \sum_{i=1}^N \sum_{r=1}^{N/2} J_r \mathbf{S}_i \cdot \mathbf{S}_{i+r}, \quad (2)$$

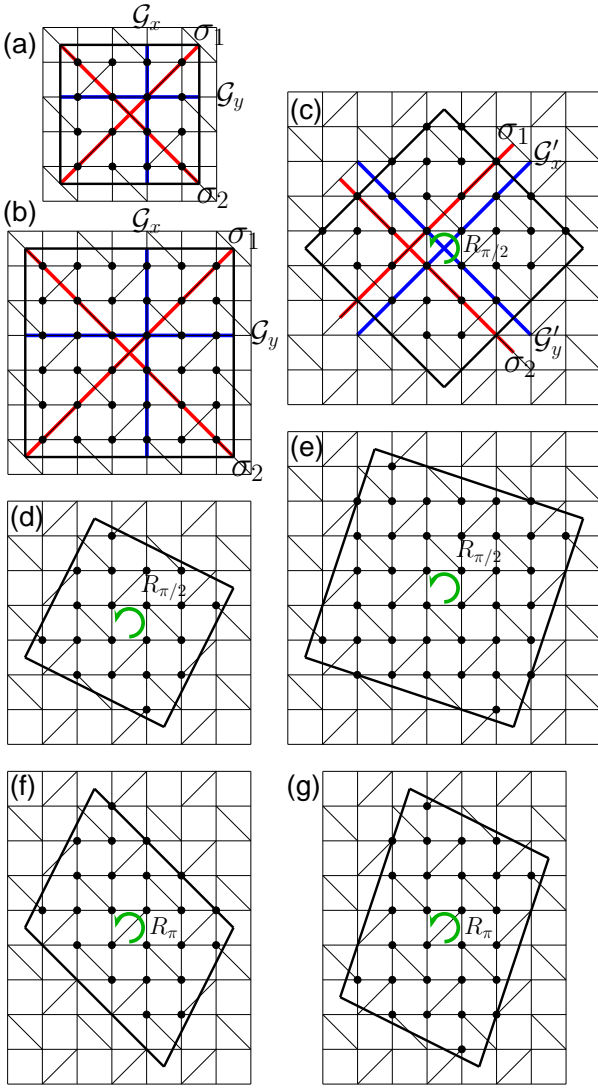


Figure 2. The seven clusters studied in this work. For each system size N , a cut-out from the infinite lattice is indicated and periodic boundary conditions are applied to these finite clusters. The clusters are arranged according to their different symmetries and the sizes N are (a) 16, (b) 36, (c) 32, (d) 20, (e) 40, (f) 24, and (g) 28, with the sites included in each cluster marked by the black circles. The lattice symmetries are illustrated as follows: Gliding reflection operators \mathcal{G}_x and \mathcal{G}_y in (a) and (b), defined in Eq. (5), involve reflection with respect to the blue lines; analogous operations \mathcal{G}'_x and \mathcal{G}'_y are defined for the cluster in (c). Mirror reflections σ_1 and σ_2 are defined with respect to the red lines in (a)-(c). Rotation R_ϕ by an angle ϕ is defined with respect to the center of an empty or filled plaquette as indicated by the green semi-circles in (c)-(g).

where the distance dependent couplings are given by [46]

$$J_2 = g, \quad J_{r \neq 2} = \frac{(-1)^{r-1}}{r^\alpha} \left(1 + \sum_{r'=3}^{N/2} \frac{1}{r'^\alpha} \right)^{-1}, \quad (3)$$

with adjustable parameters α and g and the normalization of $J_{r \neq 2}$ chosen such that the sum of all nonfrustrated ($r \neq 2$) interactions $|J_r|$ equals 1. This model has been studied in pre-

vious works using the conventional level-crossing approach with energies computed with the Lanczos method for N up to 32 [43] as well as with DMRG (in this case with fully periodic boundary conditions) with N up to 48 [33].

The existence of a gapless QSL in this 1D model is not controversial, as even the Heisenberg chain with only nearest-neighbor interactions has a disordered ground state with algebraically decaying correlations. With the long-range unfrustrated interactions, long-range AFM order stabilizes when α is below a critical value close to 2, with the exact value depending on short-distance details of H [48]. The third phase in this case is the same frustration-driven two-fold degenerate dimerized phase as in the J_1 - J_2 chain. The QSL can be expected on general grounds for some range of the model parameters to be located between the AFM and dimer phases, and this was confirmed in Refs. [33, 46]. Here we will show that the improved level crossing method that we developed for the SSM produces better results for the chain Hamiltonian Eq. (2) as well. The behavior of various gap crossing points, as the system transitions from dimerized to QSL and then to AFM, are very similar to those observed in the SSM.

Symmetries of the SSM—The lattice symmetries exploited here are illustrated in Fig. 2 for all the SSM clusters used in our study. These symmetries are used to block diagonalize the Hamiltonian along with the conserved magnetization S^z and the spin-inversion symmetry Z (the latter only for $S^z = 0$ states). We do not use the total spin S for block diagonalization, because of the complicated basis vectors in this case, but we compute S of the eigenstates after the diagonalization procedure.

We first discuss the point-group symmetries of the standard 4×4 ($N = 16$) and 6×6 ($N = 36$) clusters; see Figs. 2(a,b). These clusters have translational symmetry in the x and y lattice directions, which we define using the operators

$$\mathcal{T}_x = T_x^2, \quad \mathcal{T}_y = T_y^2, \quad (4)$$

where T_x and T_y denote the operations of translating by one lattice spacing in the respective directions. Periodic boundaries for an $L \times L$ cluster with even L imply the conditions $\mathcal{T}_x^{L/2} = \mathcal{T}_y^{L/2} = 1$.

We use the gliding reflection symmetries defined by

$$\mathcal{G}_x = T_y P_x, \quad \mathcal{G}_y = T_x P_y, \quad (5)$$

where P_x and P_y are mirror (reflection) operations with respect to vertical and horizontal lines passing through lattice sites. We also use diagonal mirror reflections σ_1 and σ_2 , defined with respect to lines drawn through intra-dimer (J') bonds. The $L \times L$ clusters are also invariant under the composite rotation defined as

$$\mathcal{R} = T_x T_y R_{\pi/2} = \mathcal{G}_x \sigma_1, \quad (6)$$

where $R_{\pi/2}$ is the 90° rotation operation, but this composite symmetry does not further reduce the size of the Hamiltonian

Table I. Quantum numbers corresponding to the various point-group and spin symmetries for the investigated low-energy states of clusters with $N = 16$, $N = 32$, and $N = 36$. All states have quantum number $+1$ (momentum zero) of the applicable translations \mathcal{T}_x , \mathcal{T}_y or \mathcal{T}'_x , \mathcal{T}'_y . The spin inversion symmetry Z is used only when $S^z = 0$.

	$\mathcal{G}_x, \mathcal{G}'_x$	$\mathcal{G}_y, \mathcal{G}'_y$	σ_1	σ_2	$\mathcal{R}, \mathcal{R}_{\pi/2}$	S^z	S	Z
S_1	1	1	1	1	1	0	0	1
S_2	-1	-1	-1	-1	1	0	0	1
T_1	-1	-1	1	1	-1	0	1	-1
T_2	1	1	-1	-1	-1	0	1	-1
Q_1	1	1	1	1	1	2	2	/

Table II. Quantum numbers of the investigated state with respect to the applicable rotations for $N = 20$, $N = 24$, and $N = 28$ clusters. All states have momentum zero.

	$R_{\pi/2} (N = 20)$	$R_{\pi} (N = 24, 28)$	S^z	S	Z
S_1	1	1	0	0	1
S_2	1	1	0	0	1
T_1	-1	1	0	1	-1
T_2	-1	1	0	1	-1
Q_1	1	1	2	2	/

blocks after the other symmetries have been used. We nevertheless compute the eigenvalue of \mathcal{R} using that of \mathcal{G}_x and σ_1 .

The $N = 32$ cluster is contained in a square that is 45° rotated with respect to the lattice axes; see Fig. 2(c). Defining \mathcal{T}'_x and \mathcal{T}'_y as translations along the diagonal directions by one step, the cluster is invariant under the following operations: $\mathcal{T}'_x = \mathcal{T}_x'^2$, $\mathcal{T}'_y = \mathcal{T}_y'^2$, $\mathcal{G}'_x = \mathcal{T}'_y P'_x$, $\mathcal{G}'_y = \mathcal{T}'_x P'_y$, σ_1 , σ_2 , and $\mathcal{R}_{\pi/2}$. Here we have defined P'_x and P'_y as mirror operations with respect to diagonal lines passing only through empty plaquettes. Imposing periodic boundary conditions corresponds to $\mathcal{T}_x'^2 = \mathcal{T}_y'^2 = 1$. For this cluster, the rotation symmetry $\mathcal{R}_{\pi/2}$ is also useful for block diagonalization.

The $N = 20$ and $N = 40$ clusters, Fig. 2(d,e), are invariant under \mathcal{T}_x and \mathcal{T}_y , and because of the tilting the periodicity implies $\mathcal{T}_x^2 \mathcal{T}_y = 1$ for $N = 20$ and $\mathcal{T}_x^3 \mathcal{T}_y = 1$ for $N = 40$. We also use the 90° rotation symmetry, $\mathcal{R}_{\pi/2}$, with respect to the center of an empty plaquette.

Finally, the $N = 24$ and $N = 28$ clusters, Fig. 2(f,g), are similar, being symmetric with respect to a 180° rotation \mathcal{R}_π about the center of a filled plaquette. The translational constraints are $\mathcal{T}_x \mathcal{T}_y^2 = 1$ and $\mathcal{T}_x^2 \mathcal{T}_y = 1$, respectively, for $N = 24$ and $N = 28$.

Characteristic SSM eigenstates—Upon increasing g , the SSM undergoes a first-order quantum phase transition between the unique DS state and the two-fold degenerate PSS state by a true level crossing at $g \approx 0.685$ [49, 50]. We here focus solely on changes in the low-energy level spectrum for $g \geq 0.7$, excluding the well understood DS phase and the trivial transition out of it. We target the quantum phase transition from the PSS ground state to the putative QSL state at

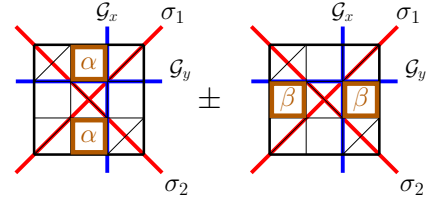


Figure 3. Cartoon picture of the \pm superpositions of α type (bold squares in the left configuration) and β type (right configuration) singlet plaquettes that form the two-fold degenerate ground states (quasi-degenerate for finite N) S_1 (+) and S_2 (−) of the PSS phase. Some of the symmetry operations used to understand (as explained in the text) the quantum numbers of the low-energy excitations T_1 , T_2 , and Q_1 are indicated with corresponding mirror lines.

$g = g_{c1} \approx 0.79$, followed by the transition from this state into the AFM state at $g = g_{c2} \approx 0.82$ [31]. Thus, we aim to understand how the low-energy spectrum changes as a function of g , as in Ref. [31] but with important differences because of the cylindrical boundary conditions used previously and the fully periodic clusters studied here.

The two-fold degenerate singlet ground state is an essential and useful feature of the PSS phase of the SSM on the fully periodic clusters studied here. We label these states, whose degeneracy is lifted by finite-size effects, as S_1 and S_2 . The characteristic Anderson rotor tower of states [51] is a hallmark of AFM order, and we consider the first two of these multiplets; the triplet excitation T_1 (which we compute in the $S^z = 0$ sector) and the quintuplet Q_1 (for practical reasons computed in the $S^z = 2$ sector). The intermediate QSL state of the SSM argued in Ref. [31] has not yet been fully characterized, and, thus, there are no rigorously known distinguishing spectral features of it. However, the results of Ref. [31] indicate that it should have gapless singlet and triplet excitations. Thus, all three phases under consideration should have gaps that vanish as the system size is increased, and we are interested in potential level crossings signaling the ground state phase transitions.

In addition to the four low-energy states S_1 , S_2 , T_1 , and Q_1 , discussed above, we also study a triplet T_2 that can be regarded as an excitation above S_2 with the same relative quantum numbers as those of T_1 relative to S_1 . All states studied here have momentum zero, i.e., the phase factor generated when applying the translation operators \mathcal{T}_x and \mathcal{T}_y in Eq. (4) to these states is $+1$. The absolute and relative lattice quantum numbers of interest here are therefore only the even ($+1$) and odd (-1) phases associated with the point-group symmetry operations. The absolute quantum numbers of the $N = 16, 32$ and $N = 36$ clusters are listed in Tab. I, and in Tab. II the applicable quantum numbers are similarly listed for $N = 20$ and $N = 24$, and 28. For $N = 40$, we have not been able to converge the target state T_2 with DMRG, but for all other states the quantum numbers are the same as those for $N = 20$.

The listed quantum numbers in Tabs. I and II can be understood with the aid of a cartoon picture of the two lowest singlet states in the PSS phase, illustrated in Fig. 3. These quasi-

degenerate ground states of a finite cluster, which do not break the two-fold order-parameter symmetry, are even (S_1) and odd (S_2) superpositions of the two different plaquette tilings (with singlets on empty plaquettes, as is the case in the SSM [50]) that we refer to as α and β . In Fig. 3, only two singlet plaquettes on empty squares are highlighted for each case (i.e., those that fit within the small 4×4 cluster). Though the SSM Hamiltonian is not bipartite, below we will also invoke the checkerboard sublattices A and B of the square-lattice sites.

First consider operation on the S_1 or S_2 state by either $\mathcal{G}_x, \mathcal{G}_y, \sigma_1$, or σ_2 on the clusters in Fig. 2. All these operations effectively exchanges the α and β sets of singlet plaquettes, therefore generate a phase (quantum number) $+1$ and -1 when acting on the S_1 and S_2 , respectively, thus explaining the corresponding quantum numbers listed in Tab. I.

To understand the quantum numbers of the triplet excitations, T_1 and T_2 , first note that a plaquette singlet can be regarded as a superposition of two parallel two-spin singlet bonds. Each singlet bond connects the A and B sublattices, thus, are odd with respect to exchanging $A \leftrightarrow B$ of the two sublattices. For a system in which the total number of singlet bonds is even, i.e., for N being an integer multiple of four (which is the case for all clusters studied here), the total product wave function of these singlets is even under $A \leftrightarrow B$. If one singlet is excited to a triplet, which is even under $A \leftrightarrow B$, such a state is anti-symmetric with respect to sublattice exchange. Note further that the operators $\mathcal{G}_x, \mathcal{G}_y$ involve $A \leftrightarrow B$ site exchange while σ_1 and σ_2 do not. Thus, the quantum number -1 of \mathcal{G}_x and \mathcal{G}_y in the T_1 state arises from swapping $A \leftrightarrow B$ because there is an odd number of remaining singlets pairs. Similarly, the quantum number $+1$ for σ_1 and σ_2 in T_1 follows because there is no sublattice swap. The same reasoning applies to the state T_2 , i.e., the triplet excitation of S_2 ; the relative sign difference in the gliding and mirror quantum numbers with respect to T_1 (Tab. I) arises from the odd superposition of the two sets α, β of plaquette tilings in S_2 .

The state Q_1 can be thought of as the result of exciting two singlet dimers of S_1 into triplets, and by applying symmetry operations as above, all reflection quantum numbers remain the same in Q_1 as in S_1 because of the even number of triplets.

The quantum numbers of the rotation operators, \mathcal{R}, R_π , or $R_{\pi/2}$, depending on the cluster, can likewise be understood in light of Fig. 3 and how the symmetry operations correspond or not to sublattice and plaquette swaps. As an example, for the $N = 32$ cluster the rotation operator $R_{\pi/2}$ swaps the A and B sublattices but not the α and β singlet plaquettes. Therefore, for the states S_1, S_2 and Q_1 , which contain an even number of singlet bonds, the quantum number is $+1$, while for T_1 and T_2 , which contain an odd number of singlets, the rotation quantum number is -1 .

The above arguments apply to all clusters in Fig. 2 with their respective applicable symmetry operations. We have explained the quantum numbers by examining a simple picture of the singlets in the PSS phase, and when moving to other phases the energy levels for the finite systems evolve continuously. The states $\{S_1, S_2, T_1, T_2, Q_1\}$ are still defined ac-

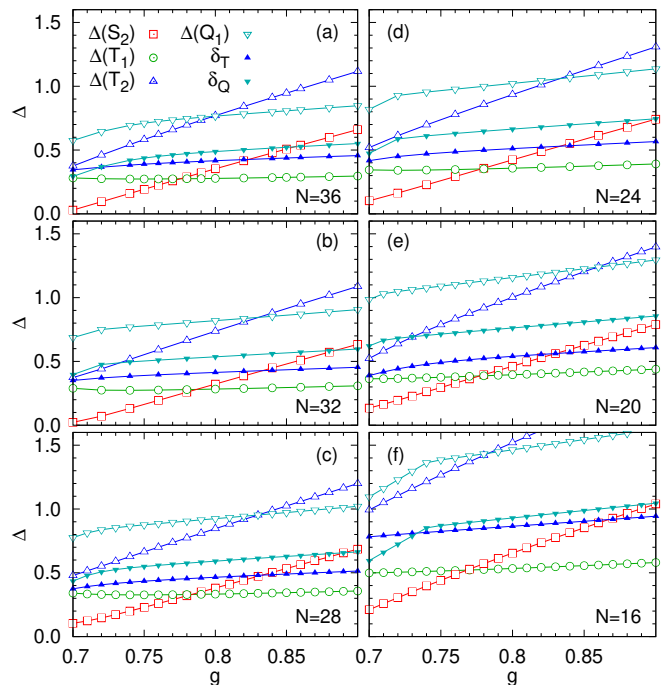


Figure 4. Energy gaps of the SSM vs the coupling for cluster sizes (a) $N = 36$ (b) 32 , (c) 28 , (d) 24 , (e) 20 , (f) 16 . Conventional gaps defined relative to the ground state energy $E(S_1)$ are shown as follows: $\Delta(S_2)$ (open red squares), $\Delta(T_1)$ (open green circles), $\Delta(T_2)$ (open blue up triangles), $\Delta(Q_1)$ (open indigo down triangles). Triplet and quintuplet gaps defined with respect to other excited states are shown as follows: $\delta_T \equiv E(T_2) - E(S_2)$ (filled blue up triangles); $\delta_Q = E(Q_1) - E(T_1)$ (filled indigo down triangles). The kinks in the $\Delta(Q_1)$ and δ_Q data between $g = 0.7$ and 0.75 are related to avoided level crossings close to the DS-PSS transition.

ording to their quantum numbers listed in Tabs. I and II and are always those that evolve from the two lowest singlets, two lowest triplets, and lowest quintuplet in the PSS state. The state S_1 remains the ground state for all values of g considered, and S_2, T_1 , and Q_1 also remain the lowest states with their respective total spin. However, T_2 is not always the second lowest triplet in the QSL and AFM phases, though it is the first triplet with its full set of quantum numbers.

Numerical SSM results—We define the gaps $\Delta(S_2), \Delta(T_1), \Delta(T_2)$, and $\Delta(Q_1)$ relative to the ground state energy $E(S_1)$ and graph these versus g in Fig. 4 for the clusters of size up to $N = 36$. As explained above, our goal is to identify level (gap) crossings with the PSS-QSL and the QSL-AFM ground state transitions.

In Ref. [31], the extrapolated (with leading $1/N$ corrections) crossing point $g_{c1} = 0.788 \pm 0.002$ between the lowest singlet and triplet excitation was identified as the PSS-QSL transition. Unlike the periodic clusters considered here, the cylindrical lattices studied in Ref. [31] break the asymptotic two-fold degeneracy of the PSS state because the boundaries favor one of the two singlet patterns. Thus, the first excited singlet was different from the quasi-degenerate ground state S_2 used here, and the level crossing studied previously is not

a directly analogy to the singlet-triplet crossing accompanying the dimerization transition in the frustrated Heisenberg chain [44, 45] (where the symmetry is not broken in periodic systems). An important aspect of the present work is that the crossing between the S_2 and T_1 levels is similar to the well understood 1D case, and a confirmation of the same asymptotic crossing point as in Ref. [31] will represent additional independent evidence for the correct identification of the quantum phase transition.

In Fig. 4, the crossing of the $\Delta(S_2)$ and $\Delta(T_1)$ gaps indeed are also close to the previous g_{c1} value for all clusters. Interpolated crossing g values are graphed versus $1/N$ in Fig. 5(a) (red squares), where we include also the $N = 40$ result obtained with the DMRG method. Here the overall size dependence is much weaker than in the cylindrical lattices [31], though there is some un-smoothness as a consequence of the different cluster shapes. A line fit to all but the $N = 16$ point gives $g_{c1} = 0.789 \pm 0.004$ (where the estimated error, here and in other extrapolations reported below, was obtained from additional fits to all data sets excluding one of the points), in remarkable agreement with the value cited above from the much larger cylindrical lattices (up to $N = 24 \times 12$ spins). The weak size dependence of the crossing points and the consistency of the two calculations illustrate the advantage of periodic boundary conditions and also confirm the quantum-critical point with a different level crossing.

The extrapolated crossing point between the lowest singlet and quintuplet excitations, $g_{c2} = 0.820 \pm 0.002$, was identified as the QSL–AFM transition [31]. This crossing point had a much larger size dependence on the cylindrical lattices than the singlet-triplet crossing. The larger size dependence is also seen with our small periodic clusters, where the crossing points between $\Delta(S_2)$ and $\Delta(Q_1)$ are outside the range of Fig. 4. The crossing values, graphed in Fig. 5(a) (indigo down triangles), are consistent with the value of g_{c2} cited above but are too scattered for a meaningful extrapolation.

Physically, the singlet-quintuplet crossing is motivated by the Anderson tower of rotor states in the AFM phase. The $S = 0$ ground state S_1 is the lowest of these states, whose gaps with respect to $E(S_1)$ scale as $S(S+1)/N$ for $S > 0$ [51]. Other singlets, including S_2 , have energies above these rotor states (for any $S > 0$ and sufficiently large N). The triplet T_1 , which becomes the $S = 1$ rotor state in the AFM phase, already crosses from above to below S_2 at the PSS–QSL transition point g_{c1} , as discussed above. There is no necessary reason why Q_1 should fall below S_2 in the QSL phase, e.g., in a scenario of a deconfined phase the quintuplet should contain four excited spinons, while S_2 and T_1 should be two-spinon excitations. However, being the $S = 2$ rotor state in the AFM phase, Q_1 has to be below S_2 there. Thus, the g value of the crossing between $\Delta(Q_1)$ and $\Delta(S_2)$ in the limit of infinite system size should coincide with the formation of AFM long-range order. The fact that the extrapolated crossing point g_{c2} indeed is larger than g_{c1} (in Ref. [31] and further below) supports an extended QSL phase instead of a direct transition point between the PSS and AFM phases.

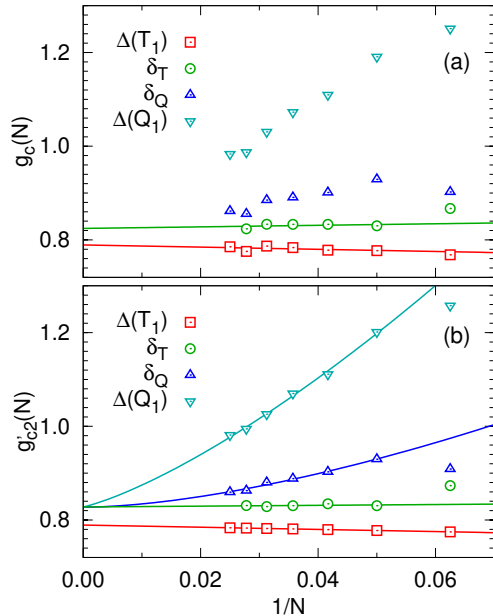


Figure 5. (a) SSM finite-size level crossing points obtained from the gaps $\Delta(T_1)$, δ_T , δ_Q , and $\Delta(Q_1)$, each crossing the singlet gap $\Delta(S_2)$. The points are graphed vs the inverse system size according to the empirical linear scaling in $1/N$ [31, 33]. The underlying data are from Lanczos calculations such as those in Fig. 4, except for the largest cluster, $N = 40$, for which the DMRG method was used. The two straight lines are fits to the $\Delta(T_1)$ (red solid line) and δ_T (green solid line) points for $N \geq 20$ and extrapolate to $g_{c1} = 0.789$ and $g_{c2} = 0.824$, respectively. (b) Adjusted crossing points, g'_{c2} , Eq. (9), for which all points for given N are shifted vertically by an equal amount so that the $\Delta(T_1)$ points (red squares) fall exactly on the red fitted line from (a). A linear fit (green line) in $1/N$ is shown for the δ_T crossing points and extrapolates to $g_{c2} = 0.826$. The form $g'_{c2}(N) = g_{c2} + a/N + b/N^{3/2}$ was fitted to the other two data sets ($N \geq 20$) with g_{c2} constrained to the same value as above.

Here our aim is to identify other gap crossings associated with the QSL–AFM transitions, in particular with the hope of reducing the size dependence and allowing reliable extrapolation of g_{c2} even with small clusters. We note that the lower transition point g_{c1} , as obtained in Ref. [31] and confirmed here, should not be controversial as it is close to other estimates of the end of the PSS phase [28, 50]—in particular, in Ref. [28] the size dependence of the point marking the upper PSS bound is consistent with our g_{c1} value.

To construct better g_{c2} estimators, we first observe that the second triplet gap $\Delta(T_2)$ in Fig. 4 closely follows the singlet gap $\Delta(S_2)$, reflecting the fact that T_2 can be regarded as a triplet excitation of S_2 , in correspondence to the role of the first triplet T_1 with respect to the ground state S_1 . Given that S_1 and S_2 are quasi-degenerate ground states in the PSS phase, the difference

$$\delta_T \equiv E(T_2) - E(S_2) \equiv \Delta(T_2) - \Delta(E_2) \quad (7)$$

will also converge with increasing system size to the non-zero gap in this phase, and δ_T must then be above the singlet splitting $\Delta(S_2)$ for sufficiently large N (as is seen clearly in Fig. 4

for all clusters). As already discussed above, in the AFM phase S_2 must be above the low-lying Anderson $S > 0$ rotor states. However, given that S_2 remains the lowest singlet excitation also in the AFM phase, it must also host long-range order and its own associated Anderson rotor tower. As T_1 is the lowest rotor excitation of S_1 , the composite excitation T_2 is the lowest rotor state excited from S_2 . Thus, in the AFM phase $\delta_T \propto 1/N$ and $\delta_T < \Delta(S_2)$, which is also seen for larger g values in Fig. 4.

In the putative gapless QSL phase, we expect S_2 to still be the lowest excited singlet (which is also found numerically) and $\Delta(S_2)$ should vanish with increasing N . Likewise, $\Delta(T_1)$ should vanish as $N \rightarrow \infty$. Both the singlet and triplet gaps were found to scale as $N^{-1/2}$ on cylinders in Ref. [31]. We also expect such scaling of the gap of T_2 relative to S_2 , i.e., $\delta_T \propto N^{-1/2}$. If δ_T remains larger than $\Delta(T_1)$ and $\Delta(S_2)$ also inside the QSL phase (as in the PSS phase), then the crossing point of $\Delta(S_2)$ and δ_T will signal the QSL–AFM transition. While we have no formal proof of this behavior, on general grounds one can expect a composite excitation, such as T_2 excited from S_2 , to be energetically more costly than its analogous elementary excitation, here T_1 obtained from the ground state S_1 .

These expectations are indeed borne out by the numerical crossing points between $\Delta(S_2)$ and δ_T in Fig. 5(a) (green circles), where we observe a surprisingly weak size dependence. Fitting a line to the data graphed versus $1/N$ for $N \geq 20$, the extrapolated QSL–AFM transition point is at $g = 0.824 \pm 0.008$, fully consistent with $g_{c2} = 0.820 \pm 0.002$ obtained previously with the larger cylindrical clusters. In this case, we do not have results for $N = 40$, as the DMRG calculation for T_2 also demands calculation of several other triplets between T_1 and T_2 (with different quantum numbers that are not resolved in our DMRG implementation [52]).

For yet another gap crossing corresponding to the QSL–AFM transition, we can construct a quantity similar to δ_T , Eq. (7), based on the quintuplet state Q_1 . In analogy with T_2 being an excitation of S_2 , we can also regard Q_1 as a further excitation of T_1 . Defining the corresponding relative gap as

$$\delta_Q \equiv E(Q_1) - E(T_1) \equiv \Delta(Q_1) - \Delta(T_1), \quad (8)$$

we can make the same kind of arguments as in the case of Q_1 and S_2 in the AFM phase, now with $\Delta(Q_1) = 3\Delta(T_1)$ asymptotically from the Anderson tower energies. Thus, asymptotically $\delta_Q \rightarrow 2\Delta(T_1)$ and we must have $\delta_Q < \Delta(S_2)$ in the AFM phase. Thus, we expect that the QSL–AFM transition is associated with the asymptotic crossing of δ_Q and $\Delta(S_2)$. Such crossing points are indeed within the range of the graphs in Fig. 4, and in Fig. 5(a) the size dependence of the crossing g values based on δ_Q (blue up triangles) is significantly reduced below that of $\Delta(Q_1)$. Visually the points are consistent with an asymptotic flow to g_{c2} , though the behavior is not smooth enough for extrapolating reliably.

An interesting observation in Fig. 5(a) is that the conventional singlet-triplet crossing points (red open squares) and the crossing of the singlet and δ_T (green open circles) are highly

correlated. Therefore, the distance between the points, i.e., asymptotically the size of the QSL phase, has much less size dependence than the individual crossing g values. Upon close inspection, such correlations are also visible in the other g_{c2} estimates. In Fig. 5(b) we exploit these correlations (which should arise from the cluster shape affecting all low-energy excitations in a similar way) by plotting points that are shifted by equal amounts up or down for given N , so that the $\Delta(T_1)$ points coincide exactly with the line fitted to those points in Fig. 5(a). In other words, we cancel out the cluster-dependent correlation effects by focusing on the relative crossing points but still taking into account the overall g scale by adding the values corresponding to the line extrapolating to g_{c1} . This procedure defines adjusted crossing points

$$g'_{c2}(N) = g_{c2}(N) - g_{c1}(N) + g_{c1}^{\text{fit}}(N), \quad (9)$$

where $g_{c1}(N)$ is the $\Delta(T_1)$ crossing point, $g_{c1}^{\text{fit}}(N)$ the corresponding value from the line fit, and $g_{c2}(N)$ is one of the other three crossing points. The so adjusted crossing points in Fig. 5(b) have much smoother size dependence. A line fit to all but the $N = 16$ data points in the case of δ_T gives $g_{c2} = 0.826 \pm 0.003$. This result is only slightly above the previous DMRG cylinder result; the calculations essentially agree within their estimated errors.

The adjusted $g'_{c2}(N)$ data sets from the $\Delta(Q_1)$ and δ_Q crossing points in Fig. 5(b) are also significantly smoothed compared to their original $g_{c2}(N)$ values in Fig. 5(a), though the visibly large corrections to the linear form, in combination with the small number of points, still make independent extrapolations with these data sets difficult. However, by fixing the $N \rightarrow \infty$ value to that obtained from the δ_T linear fits and with $1/N^{3/2}$ corrections included (corresponding to $1/L^3$ when expressed in cluster length L), the adjusted $\Delta(Q_1)$ and δ_Q data can both be fitted well, thus lending support to all three crossing points flowing to the QSL–AFM transition.

The extrapolated g_{c2} value of course also depends on the line fit to the $\Delta(T_1)$ data and its extrapolated g_{c1} value. However, the most important aspect of this analysis is that it leaves little doubt that there is a gap $g_{c2} - g_{c1} > 0$ between the two transition points, with the lines fitted to the $\Delta(T_1)$ and δ_T data only approaching each other marginally with increasing system size. It should be noted that the estimated size of the QSL phase, $g_{c2} - g_{c1} = 0.037 \pm 0.003$, is not dependent on the two individual line fits but can be obtained by a single line fit to the difference between the $\Delta(T_1)$ and δ_T points in Fig. 5(a).

Numerical results for the spin chain—Next we use the 1D frustrated spin chain Hamiltonian, Eq. (2), to further validate the conclusions drawn for the 2D SSM. In Ref. [46] the phase diagram was constructed based on Lanczos results for level crossings of gaps with respect to the ground state as well as correlation functions. In the limit of large decay exponent α of the long-range interaction, the model reduces to the well understood frustrated J_1 - J_2 chain, where a quantum phase transition between the critical ground state (a QSL of the Luttinger-liquid type) and a two-fold degenerate dimerized ground state (which we now refer to as a dimer-singlet-solid, DSS) takes

place at $J_2/J_1 \approx 0.2411$ [43–45]. For $J_2 = 0$, the interactions are not frustrated, and a previous quantum Monte Carlo and field theory study of a similar model detected a transition between the critical state and an AFM state upon lowering the long range exponent α [48]. Long-range AFM order is also intuitively expected when the interactions become strong enough at long distances so that the Mermin-Wagner theorem (which prohibits long-range AFM order for short-range interacting 1D Heisenberg systems) is no longer valid and mean-field behavior sets in. Already based on these limiting behaviors, it is clear that the phase diagram in the full parameter space (J_2, h) , where for convenience we have defined $h = \alpha^{-1}$, contains DSS, QSL, and AFM phases. These phases can be traversed in said order, similar to the phases of the SSM versus g , by following appropriate paths in the parameter space.

Based on the previous results for the phase diagram [46], we here study the phase transitions along a vertical cut with $J_2 = 0.3$ fixed and h varied. The same line in the phase diagram was also already studied with the DMRG method on periodic chains up to length $N = 48$ in Ref. [33], where level crossings of the second singlet S_2 with the first triplet (T_1) and the first quintuplet (Q_1) were extrapolated to infinite size, resulting in $h_{c1} = 0.316$ and $h_{c2} = 0.476$. We here wish to demonstrate that the finite-size effects are reduced when instead using the composite gaps defined in Eqs. (7) and (8). We only present Lanczos calculations of chains of even length N up to $N = 32$.

Figure 6 shows the four gaps relative to the ground state S_1 for chain sizes from $N = 18$ to $N = 32$. The conventional gaps $\Delta(S_2)$, $\Delta(T_1)$, $\Delta(T_2)$, and $\Delta(Q_1)$ are shown along with the two composite gaps δ_T and δ_Q defined in the same way as in Eqs. (7) and (8). Here it should be noted that chains of length $N = 4n$ (with integer n) have ground states with momentum $k = 0$, while $N = 4n + 2$ chains have $k = \pi$ (defined with translation by one lattice spacing). The arguments that we made previously based on Fig. 3 regarding the quantum numbers and physical interpretations of the low-energy states of the SSM apply also to the 1D model with its two-fold degenerate DSS in place of the PSS of the SSM, including the dependence of the ground state momentum on the chain length (from even versus odd number of singlet bonds when $N = 4n$ and $4n + 2$, respectively). We therefore do not repeat the arguments for the level crossings flowing either to the DSS–QSL transition [$\Delta(T_1)$ crossing $\Delta(S_2)$] at $h = h_{c1}$ or to the QSL–AFM transition [$\Delta(Q_1)$, δ_T , or δ_Q crossing $\Delta(S_2)$] at $h = h_{c2}$.

In Fig. 7 we present the size dependence of the relevant crossing points, graphing them versus $1/N^2$ in which case we expect asymptotic linear behavior. A clear window $h_{c2} - h_{c1} > 0$ between the extrapolated crossing points is apparent here, corresponding to the known QSL phase located between the DSS and AFM phases. Similar to the SSM, the $\Delta(T_1)$ crossing points only exhibit weak size dependence in their flow to the DSS–QSL transition at h_{c1} , here with smooth behavior as all system sizes correspond to the same shape

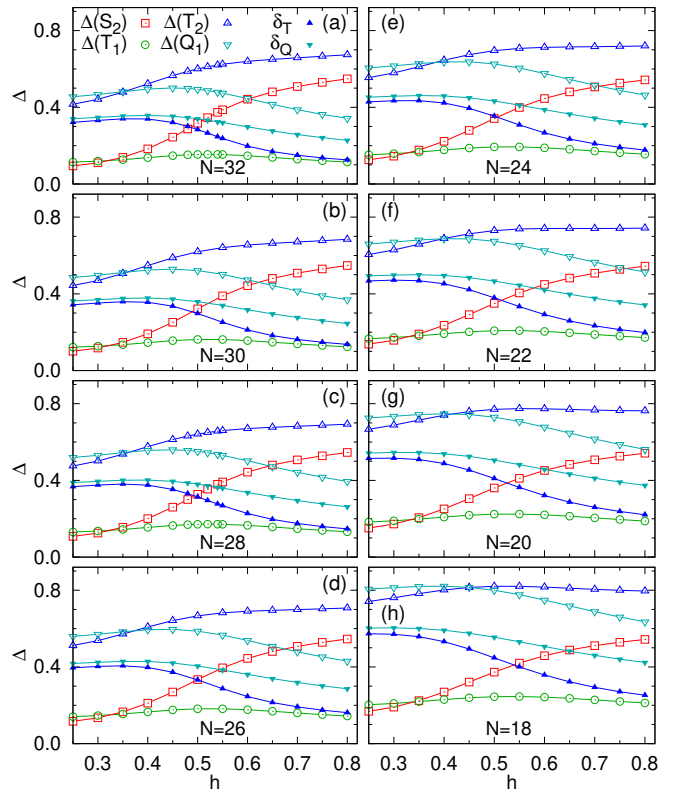


Figure 6. Energy gaps of the spin chain Hamiltonian in Eq. (2) vs the inverse of the long-range exponent $h = \alpha^{-1}$: $\Delta(S_2)$ (open red squares), $\Delta(T_1)$ (open green circles), $\Delta(T_2)$ (open blue up triangles), and $\Delta(Q_1)$ (open indigo down triangles). The composite gaps are also shown; δ_T (filled blue up triangles) and δ_Q (filled indigo down triangles), as defined in Eqs. (7) and (8), respectively. The results in (a)–(h) were obtained with the Lanczos method for chains of length $N = 32$ down to $N = 18$ in steps of 2.

of the lattice for all N . The extrapolated transition point is $h_{c1} = 0.3177 \pm 0.0002$, in good agreement with the previous results [33], where the same level crossing was used but with larger chains.

Also similar to the SSM, the weakest size dependence of the three estimates for the QSL–AFM transition point h_{c2} is achieved with δ_T , while $\Delta(Q_1)$ exhibits the largest variations with N . Thus, the use of a composite gap indeed also reduces the finite-size effects in this case. In all cases, the data for the largest clusters can be fitted with lines versus $1/N^2$, with reasonable agreement between the different extrapolations and in good agreement with the previous h_{c2} result. A constrained fit to all data sets (the lines shown in Fig. 7) with a common infinite- N point gives $h_{c2} = 0.4600 \pm 0.0005$, which is slightly lower (about 3%) than the previous DMRG result and likely more reliable.

Order parameters—We define the squared AFM (staggered) magnetization for both the SSM and the spin chain in the standard way as

$$m_s^2 = \frac{1}{N^2} \sum_{ij} \phi_{ij} \langle \mathbf{S}_i \cdot \mathbf{S}_j \rangle, \quad (10)$$

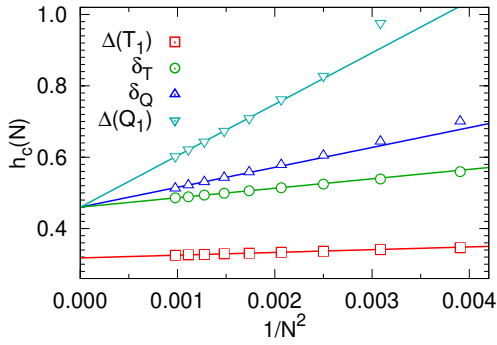


Figure 7. Finite-size crossing points extracted from the gap data in Fig. 6. The lines show fits in which a common $N = \infty$ point was enforced in the case of δ_T , δ_Q , and $\Delta(Q_1)$. Data for small N were excluded to obtain acceptable fits.

where $\phi_{ij} = +1$ and $= 1$ for sites i, j in the same and different sublattices, respectively.

The squared dimer order parameter of the chain model is defined as

$$m_d^2 = \frac{1}{N^2} \sum_{i,j} (-1)^{i-j} \langle D_i D_j \rangle, \quad (11)$$

where $D_i = \mathbf{S}_i \cdot \mathbf{S}_{i+1}$.

In the case of the SSM, singlets forming on the empty plaquettes can be detected with various operators. Here we define a plaquette operator solely with diagonal spin operators; $\Pi_i = \sigma_i^z \sigma_{i+\hat{x}}^z \sigma_{i+\hat{y}}^z \sigma_{i+\hat{x}+\hat{y}}^z$, where $\sigma_i^z = 2S_i^z$. Then

$$m_p^2 = \frac{4}{N^2} \sum_{i,j} \theta_{ij} \langle \Pi_i \Pi_j \rangle, \quad (12)$$

where i, j run only over the empty squares of the SSM lattice and $\theta_{ij} = +1$ and -1 for i, j in the same row or different rows, respectively.

Results for both order parameters of the SSM are shown in Fig. 8. While the AFM order parameter increases with g in Fig. 8(a) and the PSS order parameter m_p^2 correspondingly shows an overall reduction with g in Fig. 8(b), the signals are clearly very weak. It is not possible to extrapolate these order parameters to the thermodynamic limit, and we therefore do not show any such analysis here. In contrast, in the previous DMRG calculations [31] PSS and AFM order were clearly detected on the larger cylindrical lattices in the relevant windows of g values, and inside the QSL phase a power-law behavior of the AFM order parameter was observed. The system sizes accessible to the Lanczos method are simply too small for detecting the phase boundaries, or even to extrapolate the order parameters deep inside the PSS and AFM phases that certainly exist. We have also tried other definitions of the PSS order parameter, e.g., using cyclic permutation operators on the plaquettes instead of the diagonal operators Π_i in Eq. (12), but the g dependence is always weak, similar to the data in Fig. 8(b).

Results for the chain model are shown in Fig. 9. Here the trends versus the long-range parameter α^{-1} are clearer than in

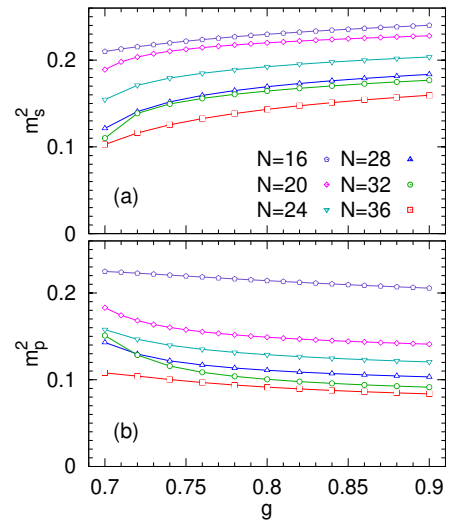


Figure 8. Squared order parameters of the SSM vs the coupling ratio for different system sizes. (a) Staggered magnetization, Eq. (10), (b) diagonal PSS order parameter, Eq. (12).

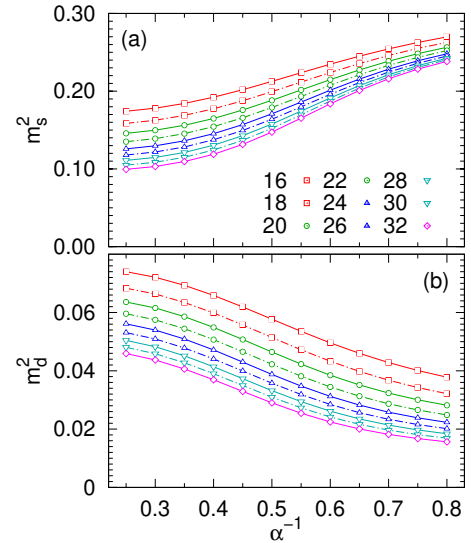


Figure 9. Squared order parameters of the chain model vs the inverse of the long-range interaction exponent. (a) Staggered magnetization, Eq. (10), and (b) dimer order, Eq. (11).

the SSM, but when contrasting the two sets of results it should be kept in mind that the system length is N in the chain but \sqrt{N} in the SSM, and the range of N is similar in both cases. The length is of course what sets the cut-off for the correlation functions and needs to be taken large to reach the asymptotic forms of the squared order parameters. Even in the 1D case, it is not possible to reliably extract the boundaries of the critical phase using the order parameters. This problem is well known from studies of the dimerization transition in the simpler J_1 - J_2 chain and was a strong impetus for the development and use of the level crossing method [43–45].

Conclusions and Discussion—Our work presented here contributes to a growing sense that level spectroscopy is one

of the most powerful generic methods for detecting quantum phase transitions, not only in the well known context of 1D models [44–46, 53, 54] but also in 2D systems [31, 33, 36, 37, 47, 55–57]. The main problem in 2D is that the accessible system sizes are typically small, and finite-size extrapolations of level crossings—the aspect of the level spectrum on which we have focused here—can be challenging. It is therefore important to extract the best possible information from the accessible level spectrum. The main conclusion on methods to draw from our study is that relative gaps between two excited states (composite excitation gaps) are useful alongside the conventional gaps relative to the ground state. In particular, the overall finite-size corrections of composite gap crossing points can be smaller. We have further shown that cluster-shape effects can be significantly removed by consider relative distances between crossing points of different gap combinations for the same system size.

The power of the level crossing method to detect quantum phase transitions is further demonstrated by the very weak signals of the different phases in the order parameters. Though the order parameters computed on larger cylinders [31] fully support the level-crossing values of the phase boundaries, on the very small lattices accessible to Lanczos diagonalization they are not yet in the asymptotic regime where the size dependence can be reliably analyzed.

The primary model studied here, the SSM, is one of the key models of quantum magnetism, yet its QSL phase situated between the PSS and AFM phases was only proposed very recently [31]. Our new results for the phase boundaries presented here are in remarkable agreement with the previous results, considering the very small clusters used, $N \leq 40$, while in Ref. [31] different gap crossings of systems with up to $N = 288$ spins were studied. Furthermore, the boundary conditions are different, fully periodic here versus cylindrical in Ref. [31]. This excellent agreement between these two different calculations suggests that the empirically found finite-size scaling behavior of gap crossing points, with leading $1/N$ corrections, is very robust and difficult to explain without the QSL phase located between the PSS and AFM phases.

For comparison, we also studied a Heisenberg chain with long-range unfrustrated interactions and short-range frustration. The initial goal of this benchmark test was to investigate the same type of level crossings used for the SSM in a system where a QSL phase located between a two-fold degenerate singlet ground state and an AFM phase is not controversial. Beyond the technical confirmation of the method, including reduced finite-size corrections when a suitable composite gap is used instead of the conventional gaps relative to the ground state, the results also contain useful information pertaining to the nature of the QSL phase in the SSM. Very similar size dependence is apparent of all the crossing points of the 1D model in Fig. 7 and the analogous points for the SSM in Fig. 5, in particular the ordering of the crossing points obtained with the different crossing gaps. This correspondence of low-energy states indicates that the two QSL phases (and critical points) have similar deconfined spinon excitations despite the differ-

ent dimensionalities, thus, they may have related field theory descriptions. We note that field theories of 2D gapless spin liquids is an active field of investigation [58–63], and the spectral information obtained here may help to determine the exact nature of the QSL phase in the SSM.

First-order direct PSS–AFM transitions have been studied in related 2D quantum spin models [30] and were previously expected also in the case of the SSM [50, 64]. The most likely generic scenario for these 2D systems is a line of first-order transitions terminating at a multi-critical deconfined quantum-critical point, after which the QSL phase opens [31, 65]. A given model may then either undergo a first-order PSS–AFM transition or cross the QSL phase, as we have argued here in the case of the SSM. We are currently exploring extended SSMs to further explore this scenario.

Recent NMR experiments on SCBO, have realized a PSS–AFM transition at low temperature, below 0.1 K, driven by the strength of an external magnetic field at high hydrostatic pressure [66]. The low transition temperature and observed scaling behaviors suggest a nearby critical point at field strength close to 6 T at a pressure slightly above 2.4 GPa (the highest pressure studied). This critical point could possibly be the deconfined quantum critical point terminating the SSM QSL phase at a finite magnetic field [31], thus motivating further studies of the QSL phase of the SSM with a magnetic field added to the Hamiltonian Eq. (1).

The SSM QSL phase at zero field may possibly be realized in SCBO somewhere between pressures of 2.6 and 3.2 GPa, where heat capacity measurements [25, 26] have not detected any phase transitions as a function of the temperature. In SCBO, a complicating factor is that the weak inter-layer couplings also will play some role [25, 29], especially when perturbing a 2D gapless phase. It would therefore also be important to study weakly coupled SSM layers.

Acknowledgments.— L.W. was supported by the National Natural Science Foundation of China, Grants No. NSFC-11874080 and No. NSFC-11734002. A.W.S. was supported by the Simons Foundation (Simons Investigator Grant No. 511064).

* lingwangqs@zju.edu.cn

† sandvik@bu.edu

- [1] Balents, L. Spin liquids in frustrated magnets. *Nature* **464**, 199 (2010).
- [2] S. Yan, D. A. Huse, and S. R. White, Spin-Liquid Ground State of the $S = 1/2$ Kagome Heisenberg Antiferromagnet, *Science* **332**, 1173 (2011).
- [3] Gapless Spin-Liquid Ground State in the Kagome Antiferromagnet H. J. Liao, Z. Y. Xie, J. Chen, Z. Y. Liu, H. D. Xie, R. Z. Huang, B. Normand, and T. Xiang. *Phys. Rev. Lett.* **118** 137202 (2017).
- [4] Y.-C. He, M. P. Zaletel, M. Oshikawa, and F. Pollmann, Signatures of Dirac Cones in a DMRG Study of the Kagome Heisenberg Model, *Phys. Rev. X* **7**, 031020 (2017).
- [5] A. Kitaev, Anyons in an exactly solved model and beyond, *Ann.*

- Phys. **321**, 2–111 (2006).
- [6] M. P. Shores, E. A. Nytko, B. M. Bartlett, and D. G. Nocera, A Structurally Perfect $S = 1/2$ Kagome Antiferromagnet, *J. Am. Chem. Soc.* **127**, 13462 (2005).
- [7] J. S. Helton *et al.*, Spin Dynamics of the Spin-1/2 Kagome Lattice Antiferromagnet $\text{ZnCu}_3(\text{OH})_6\text{Cl}_2$, *Phys. Rev. Lett.* **98**, 107204 (2007).
- [8] J. Chaloupka, G. Jackeli, and G. Khaliullin, Kitaev-Heisenberg model on a honeycomb lattice: possible exotic phases in iridium oxides A_2IrO_3 , *Phys. Rev. Lett.* **105**, 027204 (2010).
- [9] M. R. Norman, Colloquium: Herbertsmithite and the search for the quantum spin liquid, *Rev. Mod. Phys.* **88**, 041002 (2016).
- [10] P. Khuntia, M. Velazquez, Q. Barthélemy, F. Bert, E. Kermarrec, A. Legros, B. Bernu, L. Messio, A. Zorko, and P. Mendels, *Nat. Phys.* **16**, 469 (2020).
- [11] J. Zheng, K. Ran, T. Li, J. Wang, P. Wang, B. Liu, Z. X. Liu, B. Normand, J. Wen, W. Yu, Gapless Spin Excitations in the Field-Induced Quantum Spin Liquid Phase of $\alpha\text{-RuCl}_3$, *Phys. Rev. Lett.* **119**, 227208 (2017).
- [12] H. Li *et al.*, Giant phonon anomalies in the proximate Kitaev quantum spin liquid $\alpha\text{-RuCl}_3$, *Nat. Commun.* **2**, 3513 (2021).
- [13] I. Kimchi, A. Nahum, and T. Senthil, Valence Bonds in Random Quantum Magnets: Theory and Application to YbMgGaO_4 , *Phys. Rev. X* **8**, 031028 (2018).
- [14] L. Liu, H. Shao, Y.-C. Lin, W. Guo, and A. W. Sandvik, Random-Singlet Phase in Disordered Two-Dimensional Quantum Magnets *Phys. Rev. X* **8**, 041040 (2018).
- [15] H. Kawamura and K. Uematsu, Nature of the randomness-induced quantum spin liquids in two dimensions, *J. Phys.: Condens. Matter* **31**, 504003 (2019).
- [16] Y. Li, G. Chen, W. Tong, L. Pi, J. Liu, Z. Yang, X. Wang, and Q. Zhang, Rare-Earth Triangular Lattice Spin Liquid: A Single-Crystal Study of YbMgGaO_4 , *Phys. Rev. Lett.* **115**, 167203 (2015).
- [17] Z. Ma *et al.*, Spin-Glass Ground State in a Triangular-Lattice Compound YbZnGaO_4 , *Phys. Rev. Lett.* **120**, 087201 (2018).
- [18] I. Kimchi, J. P. Shekellon, T. M. McQueen, and P. A. Lee, Scaling and data collapse from local moments in frustrated disordered quantum spin systems, *Nat. Commun.* **9**, 4367 (2018).
- [19] H. Kageyama, K. Yoshimura, R. Stern, N. V. Mushnikov, K. Onizuka, M. Kato, K. Kosuge, C. P. Slichter, T. Goto, and Y. Ueda, Exact Dimer Ground State and Quantized Magnetization Plateaus in the Two-Dimensional Spin System $\text{SrCu}_2(\text{BO}_3)_2$, *Phys. Rev. Lett.* **82**, 3168 (1999).
- [20] T. Waki, K. Arai, M. Takigawa, Y. Saiga, Y. Uwatoko, H. Kageyama, and Y. Ueda, A novel ordered phase in $\text{SrCu}_2(\text{BO}_3)_2$ under high pressure, *J. Phys. Soc. Jpn.* **76**, 073710 (2007).
- [21] G. Radtke, A. Saul, H. A. Dabkowska, M. B. Salamon, and M. Jaime, Magnetic nanopantograph in the $\text{SrCu}_2(\text{BO}_3)_2$ Shastry–Sutherland lattice, *Proc. Natl. Acad. Sci.* **112**, 1971 (2015).
- [22] S. Haravifard *et al.*, Crystallization of spin superlattices with pressure and field in the layered magnet $\text{SrCu}_2(\text{BO}_3)_2$, *Nat. Commun.* **7**, 11956 (2016).
- [23] M. Zayed *et al.*, 4-spin plaquette singlet state in the Shastry-Sutherland compound $\text{SrCu}_2(\text{BO}_3)_2$, *Nat. Phys.* **13**, 962 (2017).
- [24] S. Bettler, L. Stoppel, Z. Yan, S. Gvasaliya, and A. Zheludev, Sign switching of dimer correlations in $\text{SrCu}_2(\text{BO}_3)_2$ under hydrostatic pressure, *Phys. Rev. Research* **2**, 012010(R) (2020).
- [25] J. Guo, G. Sun, B. Zhao, L. Wang, W. Hong, V. A. Sidorov, N. Ma, Q. Wu, S. Li, Z. Y. Meng, A. W. Sandvik, and L. Sun, Quantum Phases of $\text{SrCu}_2(\text{BO}_3)_2$ from High-Pressure Thermodynamics, *Phys. Rev. Lett.* **124**, 206602 (2020).
- [26] J. Larrea Jiménez *et al.*, A quantum magnetic analogue to the critical point of water, *Nature* **592**, 370 (2021).
- [27] B. S. Shastry and B. Sutherland, Exact ground state of a quantum mechanical antiferromagnet, *Physica B+C* **108**, 1069 (1981).
- [28] J. Y. Lee, Y.-Z. You, S. Sachdev, and A. Vishwanath, Signatures of a Deconfined Phase Transition on the Shastry-Sutherland Lattice: Applications to Quantum Critical $\text{SrCu}_2(\text{BO}_3)_2$, *Phys. Rev. X* **9**, 041037 (2019).
- [29] G. Sun, N. Ma, B. Zhao, A. W. Sandvik, and Z. Y. Meng, Emergent $O(4)$ symmetry at the phase transition from plaquette-singlet to antiferromagnetic order in quasi-two-dimensional quantum magnets, *Chin. Phys. B* **30**, 067505 (2021).
- [30] B. Zhao, P. Weinberg, and A. W. Sandvik, Symmetry enhanced first-order phase transition in a two-dimensional quantum magnet, *Nature Phys.* **15**, 678 (2019).
- [31] J. Yang, A. W. Sandvik, and L. Wang, Quantum criticality and spin liquid phase in the Shastry-Sutherland model, *Phys. Rev. B* **105**, L060409 (2022).
- [32] A. Keles and E. Zhao, Rise and fall of plaquette order in the Shastry-Sutherland magnet revealed by pseudofermion functional renormalization group, *Phys. Rev. B* **105**, L041115 (2022).
- [33] L. Wang and A. W. Sandvik, Critical Level Crossings and Gapless Spin Liquid in the Square-Lattice Spin-1/2 J_1 - J_2 Heisenberg Antiferromagnet, *Phys. Rev. Lett.* **121**, 107202 (2018).
- [34] S.-S. Gong, W. Zhu, D. N. Sheng, O. I. Motrunich, and M. P. A. Fisher, Plaquette Ordered Phase and Quantum Phase Diagram in the Spin-1/2 J_1 - J_2 Square Heisenberg Model, *Phys. Rev. Lett.* **113**, 027201 (2014).
- [35] S. Morita, R. Kaneko, and M. Imada, Quantum spin liquid in spin 1/2 J_1 - J_2 Heisenberg model on square lattice: Many-variable variational Monte Carlo study combined with quantum-number projections, *J. Phys. Soc. Jpn.* **84**, 024720 (2015).
- [36] F. Ferrari and F. Becca, Gapless spin liquid and valence-bond solid in the J_1 - J_2 Heisenberg model on the square lattice: Insights from singlet and triplet excitations, *Phys. Rev. B* **102**, 014417 (2020).
- [37] Y. Nomura and M. Imada, Dirac-type nodal spin liquid revealed by machine learning, *Phys. Rev. X* **11**, 031034 (2021).
- [38] H. Shackleton, A. Thomson, and S. Sachdev, Deconfined criticality and a gapless \mathbb{Z}_2 spin liquid in the square lattice antiferromagnet, *Phys. Rev. B* **104**, 045110 (2021).
- [39] N. Laflorencie and D. Poilblanc, Simulations of pure and doped low-dimensional spin-1/2 gapped systems, *Lecture Notes in Physics* **645**, 227 (2004).
- [40] R.M. Noack and S. Manmana, Diagonalization and Numerical Renormalization-Group-Based Methods for Interacting Quantum Systems, *AIP Conf. Proc.* **789**, 93 (2005).
- [41] A. Weisse, H. Fehske, Exact Diagonalization Techniques, *Lecture Notes in Physics* **739**, 529 (2008).
- [42] A. Läuchli, "Numerical Simulations of Frustrated Systems" in *Highly Frustrated Magnets*, edited by C. Lacroix, P. Mendels, and F. Mila, (Springer Verlag, 2011).
- [43] A. W. Sandvik, Computational Studies of Quantum Spin Systems, *AIP Conf. Proc.* **1297**, 135 (2010).
- [44] K. Nomura and K. Okamoto, Fluid-dimer critical point in $S = 1/2$ antiferromagnetic Heisenberg chain with next nearest neighbor interactions, *Phys. Lett. A* **169**, 433 (1992).
- [45] S. Eggert, Numerical evidence for multiplicative logarithmic corrections from marginal operators, *Phys. Rev. B* **54**, R9612 (1996).
- [46] A. W. Sandvik, Ground States of a Frustrated Quantum Spin Chain with Long-Range Interactions, *Phys. Rev. Lett.* **104**,

- 137204 (2010).
- [47] H. Suwa, A. Sen, and A. W. Sandvik, Level spectroscopy in a two-dimensional quantum magnet: Linearly dispersing spinons at the deconfined quantum critical point, *Phys. Rev. B* **94**, 144416 (2016).
- [48] N. Laflorencie, I. Affleck, and M. Berciu, Critical phenomena and quantum phase transition in long range Heisenberg antiferromagnetic chains, *J. Stat. Mech.* (2005) P12001.
- [49] A. Koga and N. Kawakami, Quantum Phase Transitions in the Shastry-Sutherland Model for $\text{SrCu}_2(\text{BO}_3)_2$, *Phys. Rev. Lett.* **84**, 4461 (2000).
- [50] P. Corboz and F. Mila, Tensor network study of the Shastry-Sutherland model in zero magnetic field, *Phys. Rev. B* **87**, 115144 (2013).
- [51] P. W. Anderson, New Approach to the Theory of Superexchange Interactions, *Phys. Rev. B* **115**, 2 (1959).
- [52] Though these triplets with energy between $E(T_1)$ and $E(T_2)$ have lattice quantum numbers different from those of T_1 and T_2 , the corresponding symmetries are not implemented in the DMRG calculation (but the total spin symmetry is implemented in this case), only computed as expectation values with the states obtained. The states have to be generated one-by-one starting from the lowest one, and convergence of this procedure becomes increasingly challenging with the number of states computed [31, 33], and we have not been able to reach the state with quantum numbers corresponding to T_2 for $N = 40$.
- [53] M. Nakamura, Tricritical behavior in the extended Hubbard chains, *Phys. Rev. B* **61**, 16377 (2000).
- [54] H. Suwa and S. Todo, Generalized Moment Method for Gap Estimation and Quantum Monte Carlo Level Spectroscopy, *Phys. Rev. Lett.* **115**, 080601 (2015).
- [55] P. Lecheminant, B. Bernu, C. Lhuillier, L. Pierre, and P. Sindzingre, Order versus disorder in the quantum Heisenberg antiferromagnet on the kagomé lattice using exact spectra analysis, *Phys. Rev. B* **56**, 2521 (1997).
- [56] G Misguich and P Sindzingre, Detecting spontaneous symmetry breaking in finite-size spectra of frustrated quantum antiferromagnets, *J. Phys.: Condens Matter* **19**, 145202 (2007).
- [57] M. Schuler, S. Whitsitt, L. P. Henry, S. Sachdev, and A. M. Läuchli, Universal Signatures of Quantum Critical Points from Finite-Size Torus Spectra: A Window into the Operator Content of Higher-Dimensional Conformal Field Theories, *Phys. Rev. Lett.* **117**, 210401 (2016).
- [58] M. Hermele, T. Senthil, and M. P. A. Fisher, Algebraic spin liquid as the mother of many competing orders, *Phys. Rev. B* **72**, 104404 (2005).
- [59] J.-Yao Chen and D. Poilblanc, Topological Z_2 resonating-valence-bond spin liquid on the square lattice, *Phys. Rev. B* **97**, 161107(R) (2017).
- [60] R. Boyack, C.-H. Lin, N. Zerf, A. Rayyan, and J. Maciejko, Transition between algebraic and F_2 quantum spin liquids at large n," *Phys. Rev. B* **98**, 035137 (2018).
- [61] E. Dupuis, R. Boyack, and W. Witczak-Krempa, Anomalous dimensions of monopole operators at the transitions between Dirac and topological spin liquids, arXiv:2108.05922.
- [62] W.-Y. Liu, J. Hasik, S.-S. Gong, D. Poilblanc, W.-Q. Chen, and Z.-C. Gu, The emergence of gapless quantum spin liquid from deconfined quantum critical point, arXiv:2110.11138.
- [63] H. Shackleton and S. Sachdev, Anisotropic deconfined criticality in Dirac spin liquids, arXiv:2203.01962.
- [64] N. Xi, H. Chen, Z. Y. Xie, and R. Yu, First-order transition between the plaquette valence bond solid and antiferromagnetic phases of the Shastry-Sutherland model, arXiv:2111.07368.
- [65] D.-C. Lu, C. Xu, and Y.-Z. You, Self-duality protected multicriticality in deconfined quantum phase transitions, *Phys. Rev. B* **104**, 205142 (2021).
- [66] Y. Cui, L. Liu, H. Lin, K.-H. Wu, W. Hong, X. Liu, C. Li, Z. Hu, N. Xi, S. Li, R. Yu, A. W. Sandvik, W. Yu, Deconfined quantum criticality and emergent symmetry in $\text{SrCu}_2(\text{BO}_3)_2$, arXiv:2204.08133.